Experimental and Theoretical Spin Density in a Ferromagnetic Molecular Complex Presenting Interheteromolecular Hydrogen Bonds

ARTICLE *in* JOURNAL OF THE AMERICAN CHEMICAL SOCIETY · OCTOBER 1999

Impact Factor: 12.11 · DOI: 10.1021/ja991042u

Experimental and Theoretical Spin Density in a Ferromagnetic Molecular Complex Presenting Interheteromolecular Hydrogen Bonds

Yves Pontillon,[†] Takeyuki Akita,[‡] Andre Grand,[§] Keiji Kobayashi,[‡] Eddy Lelievre-Berna,[||] Jacques Pécaut,[§] Eric Ressouche,[†] and Jacques Schweizer*,[†]

Contribution from the Commissariat à l'Energie Atomique, MDN/SPSMS/DRFMC, CEN-Grenoble, 17 rue des Martyrs, 38054 Grenoble Cedex 9, France, Department of Chemistry, Graduate School of Arts and Sciences, The University of Tokyo, Komaba, Meguro-Ku, Tokyo 153-8902, Japan, Institut Laue-Langevin, Av. des Martyrs, BP 156, 38042 Grenoble Cedex 9, France, and Commissariat à l'Energie Atomique, SCIB/DRFMC, CEN-Grenoble, 17 rue des Martyrs, 38054 Grenoble Cedex 9

Received April 1, 1999. Revised Manuscript Received August 18, 1999

Abstract: The association of phenylboronic acid (no unpaired electron, compound **1**) with the free radical phenyl nitronyl nitroxide (PNN, $S = {}^1/_2$, compound **2**) constitutes an interheteromolecular hydrogen bonding system displaying ferromagnetic intermolecular interactions. We have investigated its spin density distribution to visualize the pathway of these magnetic interactions. This complex crystallizes at room temperature in the monoclinic space group $P2_1/n$. The unit cell includes one pair (**1** + **2**). The molecule (**1**) bridges two radicals (**2**) by hydrogen bonds OH···ON: the two different hydrogen bond lengths are quite similar (1.95 and 1.92 Å). Infinite chains of this run along the *b*-axis. In this structure the methyl groups of the PNN are randomly distributed in two different configurations. Below $T = 220$ K the compound undergoes a crystallographic phase transition due to the ordering of these methyl groups. We have determined the low-temperature structure using both X-ray and neutron diffraction. The new space group is $P\bar{1}$. The global structure is preserved and infinite chains still run along the *b*-axis, but the unit cell now comprises two different pairs (**1** + **2**) instead of one, with four different hydrogen bond OH···ON distances: 1.96 and 1.84 Å for the first pair, 1.96 and 1.91 Å for the second pair. The spin density of this complex was measured at $T = 1.8$ K ($H = 4.6$ T) by polarized neutron diffraction. The data were treated using both maximum entropy approach and wave function modeling. As in the isolated PNN, the main part of the spin density is located on the O−N−C−N−O fragment of each radical in the unit cell. However, compared to the isolated case, a significant difference exists: a large unbalance is observed between the two oxygen atoms of each radical. Moreover, a positive contribution is found on the two hydrogen atoms involved on the OH···ON hydrogen bonds of each phenylboronic acid molecule. The stronger contribution corresponds to the longer hydrogen bonds. On the radical the stronger reduction is observed on the oxygen atoms involved in the shorter hydrogen bonds. The experimental results are compared to those obtained by density functional theory (DFT) calculations: on the whole, the experimental effects have been reproduced. However, if there is a good qualitative agreement, from the quantitative point of view, the DFT results are still very far from the experimental ones.

Introduction

Ullman's nitronyl nitroxide radicals[1] (2-substituted 4,4,5,5-tetramethyl-4,5-dihydro-1H-imidazolyl-1oxyl-3-oxide, Figure 1), first synthesized as possible spin labels, have been widely used in the preparation of metal complexes displaying ferromagnetic properties.[2] Later, it was found that these kinds of materials could by themselves present ferromagnetic order or ferromagnetic behavior at low temperature.[3] Since then, only a few compounds exhibiting these behaviors have been synthesized,[4] and some theoretical modeling works were reported.[5−7]

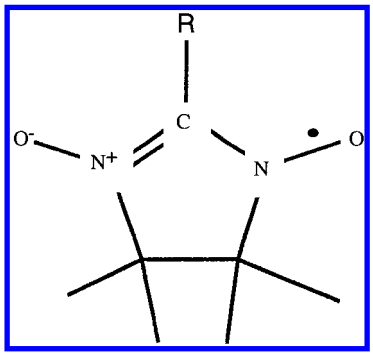

Figure 1. General formula of nitronyl nitroxide free radicals.

The macroscopic physical properties of molecular crystals are defined by intermolecular electronic interactions present in

[†] MDN/SPSMS/DRFMC. Present address for Y. Pontillon: University of Florence.
[‡] University of Tokyo.
[§] SCIB/DRFMC.
[||] Institut Laue-Langevin.

(1) Ullman, E. F.; Osieki, J. H.; Boocock, D. G. B.; Darcy, R. *J. Am. Chem. Soc.* **1972**, *94*, 7049.

(2) Caneschi, A.; Gatteschi, D.; Rey, P. *Prog. Inorg. Chem.* **1991**, *39*, 331. Caneschi, A.; Gatteschi, D.; Laugier, J.; Rey, P.; Sessoli, R.; Zanchini, C. *J. Am. Chem. Soc.* **1988**, *110*, 2795. Caneschi, A.; Gatteschi, D.; Rey, P.; Sessoli, R. *Inorg. Chem.* **1988**, *27*, 1756. Caneschi, A.; Gatteschi, D.; Sessoli, R.; Rey, P. *Acc. Chem. Res.* **1989**, *22*, 392.

(3) Awaga, K.; Maruyama, Y. *Chem. Phys. Lett.* **1989**, *158*, 556. Kinoshita, M.; Turek, P.; Tamura, M.; Nozawa, K.; Shiomi, D.; Nakazawa, M.; Ishikawa, M.; Takahashi, M.; Awaga, K.; Inabe, T.; Maruyama, Y. *Chem. Lett.* **1991**, 1225. Awaga, K.; Inabe, T.; Nagashima, U.; Maruyama, Y. *J. Chem. Soc., Chem Commun.* **1989**, 1617.

10.1021/ja991042u CCC: $18.00
Published on Web 10/13/1999

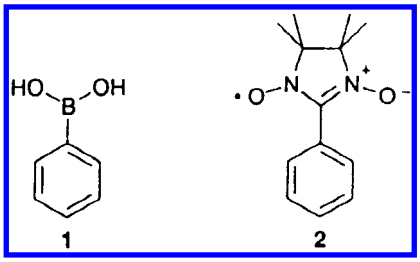

Figure 2. Chemical structure of the PNNB complex: (**1**) phenylboronic acid and (**2**) phenyl nitronyl nitroxide.

the solid state. Consequently, there is a need for the development and study of crystalline design elements producing strong and highly directional intermolecular interactions that are able to generate predetermined molecular arrangements.

The high directionality of strong (O−H···O−N) and weak (C−H···O−N) hydrogen bonds makes them useful crystalline design elements for the preparation of molecular materials with controlled properties.[8−9] Recently, it has been found[10] that both types of hydrogen bonds are able not only to control the crystal packing of open-shell molecules but also to generate and propagate ferromagnetic interactions through them. However, many of these works have been devoted to the use of interhomomolecular hydrogen bonds (IHoHB) to obtain a ferromagnetic interaction in the solid state. Another approach is the use of interheteromolecular hydrogen bonds (IHeHB) to constitute a supramolecular structure and a spin transmission path via a diamagnetic compound. The first example[11] of this type of molecular complex showing ferromagnetic intermolecular interactions was obtained with the phenylboronic acid (no unpaired electron, compound **1**, Figure 2) in association with the phenyl nitronyl nitroxide (PNN) ($S = {}^1/_2$, compound **2**, Figure 2), referred to herein as PNNB.

We have shown, for one of the IHoHB radicals, that hydrogen bonds play a major role in the propagation of magnetic interactions.[12−13] We report here an investigation of the role of the hydrogen bonds in the transmission of ferromagnetic interactions in a IHeHB molecular complex. This paper includes the low-temperature crystal structure determination (X-ray diffraction) and the experimental (polarized neutron diffraction) and the theoretical (ab initio calculations) spin density study of PNNB. The latter results are compared to those obtained previously for the "isolated" PNN radical,[14] which is paramagnetic. We derive here important magnetostructural correlations, considering the role played by the crystal packing and the phenylboronic acid in the redistribution of the spin density within the radical and, consequently, in the intermolecular exchange pathway.

Several possible mechanisms leading to ferromagnetic coupling between the nitronyl nitroxide radicals were proposed, but experimental evidence has been controversial, and statistical elaborations have so far been unsuccessful to provide unequivocal evidence as to which are the most efficient pathways leading to ferromagnetic coupling. One problem is that the magnetic interactions are often very weak, and so we decided to measure the spin density distribution by polarized neutron diffraction to substantiate qualitative conclusions.

Polarized neutron diffraction is a very powerful technique for spin density studies in magnetic molecular materials.[15] The measurements are usually performed in the paramagnetic state. The spin density $S(\vec{r}) = S(r)\hat{z}$ is induced in a single-crystal sample by applying a strong external magnetic field ($\hat{z}$ being the field direction) at low temperature (in practice below 5 K) to maximize the amount of ordered spin density induced by the applied field. By using a polarized beam, one measures the flipping ratios R of Bragg reflections (hkl), which is the ratio of scattered intensities for "up" (parallel to the applied field, $I^{\uparrow}$) and "down" (antiparallel, $I_{\downarrow}$) polarizations of the incident beam. If the crystal structure is centrosymmetric, the nuclear and magnetic structure factors F_N and F_M are real quantities, and the flipping ratios are related to the magnetic structure factors F_M, the spatial Fourier components of $S(r)$, by the following expression:

$$R_{(h,k,l)} = \frac{I^{\uparrow}}{I_{\downarrow}} = \frac{F_N^2 + F_{M\perp}^2 + 2F_N F_{M\perp z}}{F_N^2 + F_{M\perp}^2 - 2F_N F_{M\perp z}} \qquad (1)$$

$$F_{M\perp} = F_M \sin\alpha \qquad F_{M\perp z} = F_M \sin^2\alpha$$

where α is the angle between the scattering vector (hkl) and $\vec{z}$. The F_M's may be directly deduced from the experimental flipping ratios if the crystal structure of the compound is known.[15] Thus, the experiment generally consists of two steps. In the first one, the precise structure of the crystal at low temperature, including the location of the hydrogen atoms and the determination of the thermal parameters, is investigated using conventional unpolarized neutron diffraction techniques. The second step consists of measuring the flipping ratios with polarized neutrons.

In the present case, the usual procedure was started. However, during this first step it appeared that, on cooling, the compound undergoes a crystallographic phase transition at $T = 220$ K with a loss of symmetry. As a consequence, the large crystal that was used for that unpolarized neutron experiment splits in several subcrystals at the transition and no crystal structure could

(4) Chiarelli, R.; Novak, M. A.; Rassat, A.; Tholence, J. L. *Nature* **1993**, *363*, 147. Sugano, T.; Tamura, M.; Kinoshita, M.; Sakai, Y.; Ohashi, Y. *Chem. Phys. Lett.* **1992**, *200*, 235. Turek, P.; Nozawa, K.; Shiomi, D.; Awaga, K.; Inabe, T.; Maruyama, Y.; Kinoshita, M. *Chem. Phys. Lett.* **1991**, *180*, 327. Hosokoshi, Y.; Tamura, M.; Kinoshita, M. *Mol. Cryst. Liq. Cryst.* **1993**, *232*, 45.

(5) Fang, Z.; Liu, Z. L.; Yao, K. L. *Phys. Rev. B* **1994**, *49*, 3916 and *Phys. Rev. B* **1995**, *51*, 1304.

(6) Wang, W. Z.; Liu, Z. L.; Yao, K. L. *Phys. Rev. B* **1997**, *55*, 12989 and *J. Chem. Phys.* **1998**, *108*, 2868.

(7) Bencini, A.; Ciofin, I.; Giannasi, E.; Daul, C. A.; Doclo, K. *Inorg. Chem.* **1998**, *37*, 3719. Yamanaka, S.; Kawakami, T.; Yamada, S.; Nagao, H.; Nakano, M.; Yamaguchi, K. *Chem. Phys. Lett.* **1995**, *240*, 268. Awaga, K.; Maruyama, Y. *J. Chem. Phys.* **1989**, *91*, 2743. Delley, B.; Becker, P.; Gillon, B. *J. Chem. Phys.* **1984**, *80*, 4286.

(8) Etter, M. *J. Phys. Chem.* **1991**, *95*, 4601. Brown, I. D. *Acta Crystallogr., Sect. A* **1976**, *32*, 24.

(9) Taylor, R.; Kennard, O. *Acc. Chem. Res.* **1984**, *17*, 320. Desiraju, G. R. *Acc. Chem. Res.* **1991**, *24*, 290.

(10) (a) Cirujeda, J.; Ochando, L. E.; Amigo, J. M.; Rovira, C.; Rius, J.; Veciana, J. *Angew. Chem., Int. Ed. Engl.* **1995**, *34*, 55. Cirujeda, J.; Mas, M.; Molins, E.; de Panthou, F. L.; Laugier, J.; Park, J. G.; Paulsen, C.; Rey, P.; Rovira, C.; Veciana, J. *J. Chem. Soc., Chem. Commun.* **1995**, 709. Sugawara, T.; Matsushita, M.; Izuoka, A.; Wada, N.; Takeda, N.; Ishikawa, M. *J. Chem. Soc., Chem. Commun.* **1994**, 1723. Okuno, T.; Otsuka, T.; Awaga, K. *J. Chem. Soc., Chem. Commun.* **1995**, 827. Romero, F. M.; de Cian, A.; Fisher, J.; Turek, P.; Ziessel, R. *New J. Chem.* **1996**, *20*, 919.

(11) Akita, T.; Mazaki, Y.; Kobayashi, K. *J. Chem. Soc., Chem. Commun.* **1995**, 1861.

(12) Romero, F. M.; Ziessel, R.; Bonnet, M.; Pontillon, Y.; Ressouche, E.; Schweizer, J.; Grand, A.; Paulsen, C. *J. Am. Chem. Soc.*, in press.

(13) Pontillon, Y.; Ressouche, E.; Romero, F.; Schweizer, J.; Ziessel R. *Phys. B* **1997**, *234−236*, 788.

(14) Zheludev, A.; Barone, V.; Bonnet, M.; Delley, B.; Grand, A.; Ressouche, E.; Rey, P.; Subra, R.; Schweizer, J. *J. Am. Chem. Soc.* **1994**, *116*, 2019.

(15) Gillon B.; Schweizer J. J. Study of Chemical Bonding in Molecules: The interest in Polarised Neutron Diffraction. In *Molecules in Physics, Chemistry and Biology*; Jean Maruani, Ed.; Kluwer Academic Publisher: Dordrecht, The Netherlands, **1989**; Vol. II, p 111.

Table 1. Crystal Data at Room Temperature, 143 K (X-ray Diffraction) and 5 K (Neutron Diffraction), Together with the Experimental Parameters for the 143 K X-ray Diffraction Experiment

temperature	room temp.	143 K	5 K
space group	$P2_1/n$	$P\bar{1}$	$P\bar{1}$
a	14.764 (3) Å	14.5322 (1) Å	14.50 (1) Å
b	9.482 (3) Å	9.3596 (2) Å	9.3596 Å[a]
c	13.686 (2) Å	13.6398 (2) Å	13.66 (2) Å
α	90	92.079 (1)°	92.079° [a]
β	90.20 (1)°	90.234 (1)°	89.75 (9)°
γ	90	91.263 (1)°	91.263° [a]
V	1915.9 (7) Å^3	1853.53 (5) Å^3	1851.18 Å^3
Z	4	2	2
		data collection (143 K)	
		8313 refl. col.	
		6157 ind.refl. ($I > 2\sigma I$)	
		$\lambda = 0.7107$	
		θ: 1.40°−25.99°	
		662 parameters	
		$wR(F^2) = 7.11\%$	

[a] Parameters not refined.

be determined on it. A tentative experiment to pass the 220 K transition on a very small crystal, suitable for X-ray diffraction, happened to be successful: below this temperature this small sample remained a single crystal and it was possible to perform an X-ray diffraction experiment and to determine the low-temperature structure of this compound ($T = 143$ K).

Since this paper includes two different parts (structural study and spin density determination), we shall present successively these two studies.

Crystal Structure Study

The synthesis and the magnetic properties of the PNNB molecular complex were already described.[11,16] Crystals suitable for the experiments were obtained by recrystalization of **1** from a mixture of hexane and dichloromethane with **2**. The room-temperature crystal structure is known from preliminary X-ray diffraction.[11] There is one pair of molecules (**1** + **2**) in the unit cell. These pairs are arranged in such a way that each of the components are connected by hydrogen bonds between the NO groups of **2** and the OH groups of **1**. Thus, the radical species **2** is arranged alternately with phenylboronic acid **1** to make an infinite chain of ···**1**···**2**···**1**···**2**··· via hydrogen bonds NO···HOB. Moreover, the four methyl groups of the five-membered ring exhibit disorder.[11] The corresponding crystal parameters are reported in Table 1.

As described in the Introduction, the PNNB complex undergoes a crystallographic phase transition at $T = 220$ K. Consequently, we have investigated this new structure with both X-ray and neutron diffractions.

Low-Temperature X-ray Crystallography. A very small crystal of size 0.2 × 0.1 × 0.05 mm^3 was analyzed using a Siemens SMART CCD area detector three-circle diffractometer (Mo Kα radiation, graphite monochromator, $\lambda = 0.71073$ Å). The cell parameters were obtained with intensities detected on three batches of 15 frames with a 10 s exposure time for several temperatures between room temperature and 143 K. The values of the cell parameters as function of temperature show that there is a phase transition for $T \approx 220$ K: the angles α and *γ* increase from 90° to ≈ 92° and ≈ 91° respectively (Figure 3). However, this very small sample remained a single crystal. Consequently, it was possible to solve the new crystal structure at $T = 143$K.

At 143 K and for three settings of Φ and 2Θ, 1200 narrow data frames were collected for 0.3° increments in *ω*. A full hemisphere of data was collected. Unique intensities with $I > 10\sigma(I)$ detected on all frames using the SAINT program[17] were used to refine the values of the cell parameters. The space group $P\bar{1}$ was determined. The structure was solved by direct methods using the SHELXTL 5.03 package,[18] and all atoms were found by difference Fourier syntheses. All nonhydrogen atoms were anisotropically refined on F^2, and hydrogen atoms were isotropically refined. Complete information on the crystal data and data collection is given in Table 1 ($T = 143$ K). Atomic coordinates, interatomic distances, bond angles, and thermal parameters (non-hydrogen atoms and hydrogen atoms) of the four independent molecules at $T = 143$ K are deposited as Supporting Information (Tables S1−S5, respectively). Figures 4 and 5 (a and b) show the independent molecules of the unit cell with the atom labeling used throughout the paper and the crystal packing, respectively ($T = 143$ K).

The transition happened to be a result of the ordering of the methyl groups of **2** (**2′**) at low temperature. The space group changes from $P2_1/n$ (room temperature) to $P\bar{1}$ (below 220 K). Consequently, below 220 K, the asymmetric unit includes two different pairs of molecules: two nitronyl nitroxyde radicals and two phenylboronic acid molecules (Figure 4). Even though the global arrangement of the molecules in the cell is only slightly different from the arrangement at room temperature, the radicals still alternate with phenylboronic acid to make an infinite chains of ···**1**···**2**···**1′**···**2′**··· along the *b*-axis via hydrogen bonds NO···HOB. The corresponding hydrogen bond distances, which were almost equivalent at room temperature, are now quite different: 1.96, 1.84, 1.96, and 1.91 Å for H24···O2, H3···O1, H4···O21 and H23···O22, respectively (Figure 5a). The corresponding torsion (*T*) and O−H···O (α) angles (see below) are, respectively, −155.32°, 102.87°, −164.70°, 100.08° and 167.84°, 175.61°, 173.91, 176.27°.

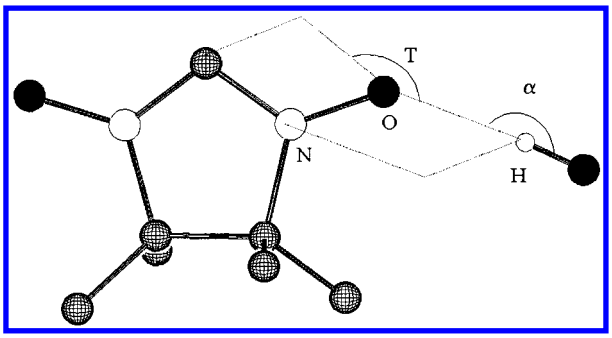

Thus, the hydrogen bonds can be grouped in two sets, one comprising the longer, whose torsion angle is in the order of 160°, and the other comprising the shorter, whose torsion angle is in the order of 100°. On the other side, the N−O bond lengths are also affected by the geometry of the hydrogen bond. The N−O distances of nitroxide groups that are involved in the longer hydrogen bonds are smaller than the others: 1.273(1), 1.284(1), 1.286(1), and 1.290(1) Å for N2−O2, N1−O1, N21−O21, and N22−O22, respectively. Moreover, as observed at room temperature, the boron atoms of molecules **1** and **1′** form planar trivalent bonds, and their phenyl substituents are almost coplanar with the trivalent boron moieties: the twist angles are only 6°. The phenyl rings of **2** and **2′** are not coplanar with the nitronyl nitroxide O−N−C−N−O plane and form an angle of 36.6° (C8−C13) and 32.7° (C28−C33). In the uncomplexed PNN, the corresponding dihedral angle is 30°.[14]

Unpolarized Neutron Diffraction. As described above, for the calculation of the F_M's from the flipping ratio measurements, a detailed knowledge of the crystal structure at the temperature where the polarized neutron experiment is performed is required. A single crystal, in the form of a regular slab of dimension 6.0 × 1.0 × 1.0 mm^3, preliminarily oriented by Laue X-ray diffraction, was used for this experiment (conventional neutron diffraction, D15 lifting counter diffractometer, ILL's reactor (Grenoble, France)). The larger edge was the [010] direction. The crystal was mounted in a cryostat such that this direction was vertical (perpendicular to the beam direction) and was cooled to 5 K. The evolution of the width of several reflections, (012), (112), ($\bar{2}$02), and (101), as a function of temperature shows that the phase transition

(16) The analysis of the χT versus T curve, between 1.8 K and room temperature,[11] with a Heisenberg chain model of $S = 1/2$ spin, yielded a ferromagnetic intrachain coupling constant $J_1 = 0.65$ K and an antiferromagnetic interchain coupling constant $J_2 \approx -0.4$ K.

(17) *Software package for use with the SMART diffractometer*; Siemens Analytical X-ray Instrument Inc.: Madison, WI, 1995.

(18) Sheldrick, G. M. *SHELXTL-Plus*, 5th ed.; Sheldrick, G. M., Ed.; University of Göttingen, Germany: Germany, 1994.

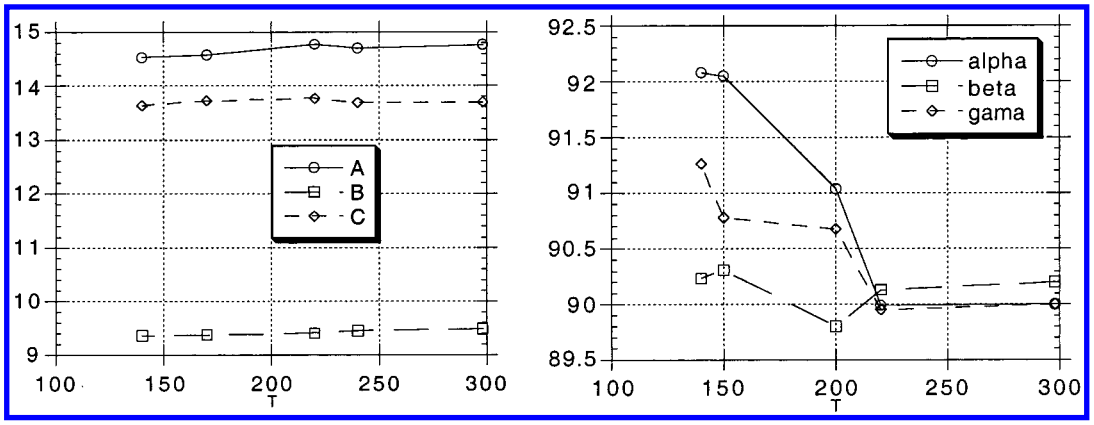

Figure 3. Evolution of the cell parameters as function of temperature (X-ray diffraction).

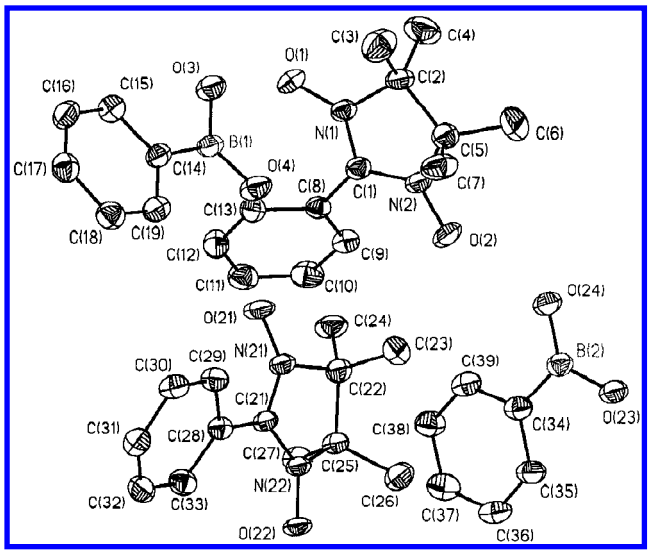

Figure 4. View of the independent molecules in their crystal geometry at $T = 143$ K with the numbering scheme of the atoms.

around 220 K is accompanied by a twinning of this crystal: only the reflections of type (*h*0*l*) are untwinned (Figure 6a). All of the other reflections are twinned; a characteristic profile of these Bragg peaks, before and after the transition, is given Figure 6b. Consequently, we have only collected reflections in the (a, c) plane. In these conditions, 346 independent Bragg intensities were measured with sin θ/λ up to 0.74 Å^{-1} ($\lambda = 1.173$ Å). The cell constants were determined to be $a =$ 14.50(1) Å, $b = 9.3596$ Å (not refined), $c = 13.66$ (2) Å, $\alpha = 92.079°$ (not refined), $\beta = 89.75$ (9)°, and $\gamma = 91.263°$ (not refined). The calculation of integrated intensities from the ω-scans was done by the COLL5 program[19] during the experimental run time. For the averaging of equivalent reflections, the program ARRNGE based on the Cambridge Crystallographic Library[20] was used. As a consequence of the restricted measurement to (*h*0*l*) reflections, only the *x* and *z* atomic positions were refined, starting from the low-temperature X-ray values, with the least-squares program ORXFLS[21] using isotropic thermal factors for all atoms. Absorption corrections were made by calculating the mean crystal path for each reflection. Extinction turned out to be significant. It was modeled in the approximation of Gaussian mosaic crystal.[22] A value of $\chi^2 = 2.1$ (weighted *R* factor = 4.9%) was achieved. The corresponding x' and z' atomic positions, together with the isotropic thermal factors, are given in Table S6 (Supporting Information).

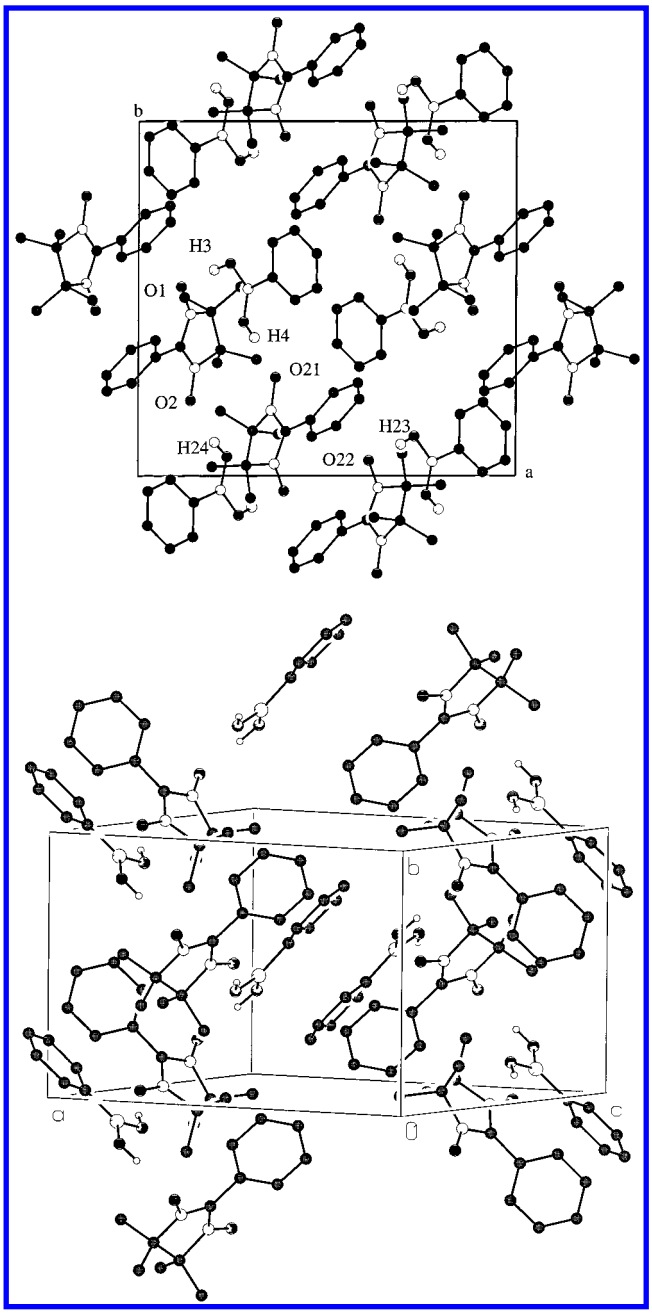

Figure 5. Crystal packing of the PNNB at $T = 143$ K: (a) projection of the crystal structure along the *b*-axis, and (b) visualization of the chains along the *b*-axis.

(19) Lehmann, M. S.; Larsen, F. K. *Acta Crystallogr., Sect. B* **1970**, *26*, 1198.

(20) Brown, P. J.; Mattheman, J. C. *The Cambridge Crystallographic Subroutine Library*; RL-81-063.

(21) Busing, W. R.; Martin, K. O.; Levy, H. A. Rapport O. R. N. L. 59−37; Oak Ridge National Laboratory: Oak Ridge, TN, 1991.

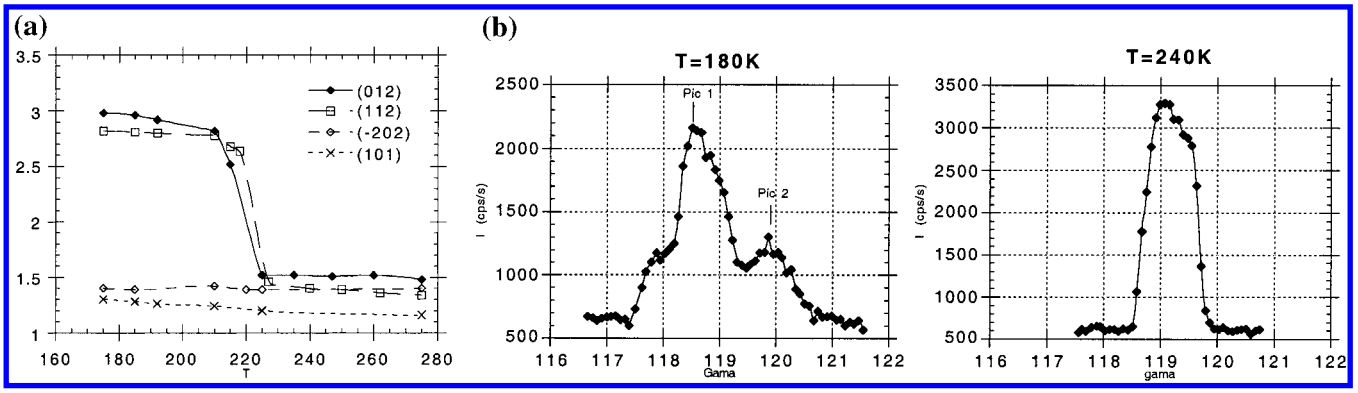

Figure 6. (a) Width evolution of reflections (012), (112), (−202), and (101) as function of temperature. (b) Profil of the reflections of type (*h*0*l*) above and below 220 K.

Spin Density Determination

The experiment was performed on the same crystal that we used in the unpolarized neutron diffraction experiment on the D3 polarized neutron lifting counter spectrometer at the ILL reactor. A beam of wavelength $\lambda = 0.843$ Å and polarization of 94% (Heussler alloy monochromator) were used. The $\lambda/2$ beam contamination was 0.3%. The crystal was mounted with the *b*-axis collinear to the 4.6 T field of a split-coil cryomagnet. Because of the twinning of the crystal due to the crystallographic transition, only the reflections of general index (*h*0*l*) are unique for all the subcrystals; all of the other Bragg peaks are a mixing of different indices and cannot be used for the spin density reconstruction. Thus, one series of measurements was carried out: 45 independent flipping ratios of type (*h*0*l*) were collected ($T = 1.5$ K for $\sin\theta/\lambda$ up to 0.35 Å^{-1}). The subroutine library mentioned above[20] was used to sort and average the equivalent flipping ratios. The precise nuclear structure factors were calculated from the low-temperature crystal structure determined by unpolarized neutron diffraction (5 K). The expression (1) for the flipping ratios was modified to include corrections due to the imperfections of the beam, the nuclear polarization of hydrogen atoms, and extinction. The magnetic structure factors F_M were calculated from this modified expression.

To obtain the (000) magnetic structure factor, an $M(T)$ curve in a field of 4.60 T (polarized neutron experimental condition) was also measured with a SQUID magnetometer. For a temperature $T = 1.5$ K at which the flipping ratios were collected, the magnetization was found to be 0.976 μ_B/PNNB complex.

Data Treatment and Results

The reconstruction of the spin density distribution $S(r)$ from the magnetic structure factors $F_M(hkl)$ is a typical Inverse Fourier (IF) problem. For the solution of this IF problem, two different approaches exist: (i) the methods where the spin density is reconstructed without any assumption on its nature (the so-called "Model-Independent Spin Density Reconstruction" techniques); and (ii) the methods based on the modeling of the spin density.

Model-Independent Spin Density Reconstruction. A straightforward inverse Fourier method is the direct application of the inverse Fourier series.[23] A much better approach is the use of the Maximum of Entropy (MaxEnt) technique,[24] which selects among all the maps consistent with the experimental data the one with the highest *intrinsic probability*, that is, the one which maximizes the configuration entropy of the map.[25]

Here, since we have measured reflections of type (*h*0*l*) only, the reconstructed spin density map is the projection onto the (a, c) plane (64 × 64 array of pixels). The calculation was performed using a program based on the MEMSYS subroutine package.[26] The resulting spin distribution is presented in Figure 7.

As previously observed in the isolated PNN,[14] the majority of the spin density is located on the O−N−C−N−O fragments of each radical included in the asymmetric unit. However, compared to the isolated case, several features need to be pointed out. (i) The spin density is not equally shared between the four atoms of the two NO groups of each radical: a strong unbalance is observed between the two oxygen atoms: the spin density on O2 (O21) is larger than on O1 (O22). (ii) A positive contribution is observed on the hydrogen atoms H4 and H24. (iii) Finally, some spin density is detected on the methyl groups of the five membered ring. No spin density is visible on the other atoms.

As it is known that MaxEnt method[14,24] hardly sees the very weak densities, we have applied the other approach to extract information on the spin density on the HOBOH fragment.

(22) Coppens; Hamilton. *Acta Crystallogr., Sect. A* **1970**, *26*, 71. Herein the formula (2) for the scattering intensity corresponding to secondary type II extinction was utilized.

$$I(k) \propto y(k)\, F^2, \text{ with } y(k) = \frac{1}{\sqrt{1 + \dfrac{2gL\lambda^3}{V^2 \sin^2\theta} F^2}} \qquad (2)$$

with V, the unit cell volume and L, the mean crystal path. The value of the coefficient g was refined together with the crystal structure ($g = 14$ (1) with L, λ, V, and F^2 in cm, Å, Å^3, and barns respectively).

(23)

$$S(x,y,z) = 1/V \sum_{h,k,l} F_M(h,k,l) e^{-2\pi i(hx+ky+lz)} \qquad (3)$$

where V is the unit cell volume. This formula is exact when the summation includes all the h, k, and l indices from $-\infty$ to $+\infty$. Practically, this method is applied with a truncated summation reduced to the reflections which have been experimentaly measured. As a result of this incomplete and arbitrary sampling of data points in the reciprocal space, the spin density maps obtained by this way are deeply biased.

(24) Papoular, R. J.; Gillon, B. *Europhys. Lett.* **1990**, *13*, 429. Papoular, R.; Zheludev, A.; Ressouche, E.; Schweizer J. *Acta Crystallogr., Sect. A* **1995**, *51*, 295.

(25) Practically, the method consists of maximizing the entropy functional (4) under the constraint $\chi^2 \leq 1$. The results are much better than the Fourier inversion series, and this method is also model-independent.

$$\text{entropy } (S(\vec{r})) = -\int_{\text{unit cell}} s(\vec{r}) \ln(s(\vec{r}))\, d^3\vec{r}$$

$$\text{with } s(\vec{r}) = \frac{S(\vec{r})}{\displaystyle\int_{\text{unit cell}} S(\vec{r})\, d^3\vec{r}} \qquad (4)$$

see Gull S. F.; Daniell G. J. *Nature* 272, **1978**, 686. Skilling J.; Gull S. F. In *Maximum Entropy and Bayesian Methods in Inverse Problems*; Smith, C. R., Grandy, W. T., Jr., Eds.; Reidel: Dordrecht, The Netherlands, 1985.

(26) Gull, S. F.; Skilling, J. *MEMSYS Users Manual*; Maximum Entropy Data Consultants Ltd, 33 North End, Meldreth, Royston SG8 6NR, England, 1989.

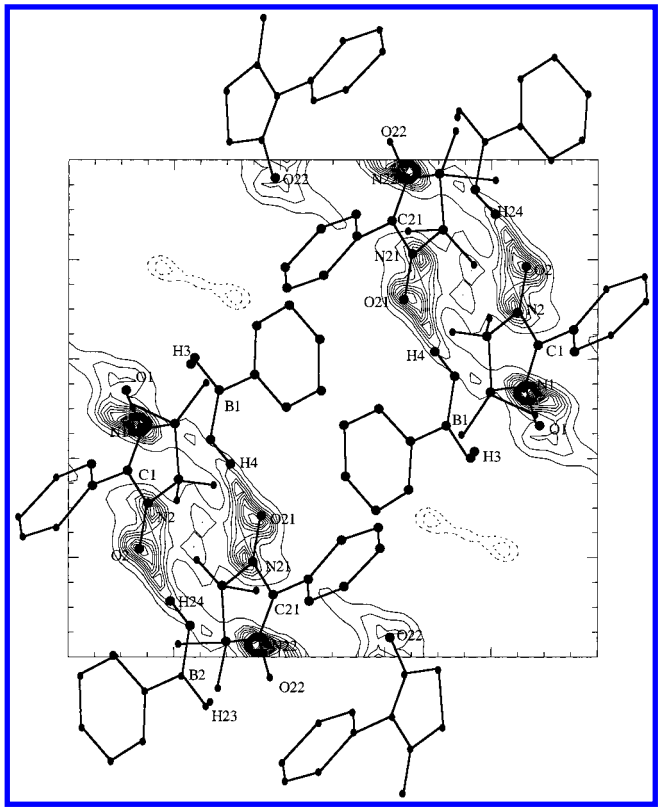

Figure 7. Projection of the MaxEnt reconstructed spin density of the PNNB onto the ($\vec{a}$, $\vec{c}$) plane. Negative contours are dashed, contour step 0.03 μ_B/Å^2.

Methods Based on the Modeling of the Spin Density. Another technique to solving the IF problem is to represent the spin density by a parametrized model and to refine the parameters of the model to best fit the experimental magnetic structure factors. Among all the possible methods, the magnetic wave function modeling is especially well adapted to treating spin densities in organic free radicals.[15] In this framework the spin density $S(\vec{r})$ is expanded as

$$S(\vec{r}) = \sum_i S_i \Psi_i(\vec{r}) \Psi_i^*(\vec{r}) \qquad (5)$$

where the sum is taken over all the atoms i included in the refinement. The S_i are the atomic spin populations and the $|\Psi_i\rangle$ are the standard Slater atomic orbitals at site i. The populations S_i as well as the radial exponents, ζ, of the Slater wave functions for each orbital type are the parameters of the model.[27]

In the particular case of the PNNB complex, only the ONCNO and HOBOH atoms of each pair were included in the refinement. $|2p_z\rangle$ orbitals centered on the O1, N1, C1, N2, and O2 (first radical) and on the O21, N21, C21, N22, and O22 (second radical) were used. The spin density on the HOBOH atoms of the phenylboronic acids is weak and is reduced to its spherical atomic contribution.

The model was refined using a least-squares method included on a modification of the MOLLY[28] program. The Slater radial exponent values were taken from literature.[29] An agreement $\chi^2 = 2.4$ value was obtained. The corresponding spin populations, together with the radial exponents ζ, are displayed in Table 2.

(27) One can note that, in this model, the $|\Psi_i\rangle$ are first squared, and only then a linear combination is made. Consequently, according to the sign of S_i, the model allows negative spin populations.

(28) Hansen, N. K.; Coppens, P. *Acta Crystallogr., Sect. A* **1978**, *34*, 909.

(29) Hehre, N. J.; Stewart, R. F.; Pople, J. A. *J. Chem. Phys.* **1969**, 51.

Table 2. Experimental Spin Populations Obtained Using the Wave Function Modeling, Together with the Slater Exponents

atoms	spin populations (μ_B)	atoms	Spin populations (μ_B)	ζ (not refined)
H3	0.024 (35)	H23	0.014(22)	(O): 2.25
O3	−0.020 (24)	O23	−0.051 (34)	(N): 1.95
B1	−0.067 (45)	B2	−0.037 (25)	(C): 1.72
O4	−0.034 (26)	O24	0.005 (26)	(B): 1.45
H4	0.043 (22)	H24	0.055 (25)	(H): 1.25
O21	0.284 (24)	O2	0.322 (25)	
N21	0.234 (24)	N2	0.242 (25)	
C21	−0.040 (23)	C1	−0.025 (20)	
N22	0.301 (22)	N1	0.301 (25)	
O22	0.210 (22)	O1	0.223 (25)	
sum	1.964			
χ^2	2.4			

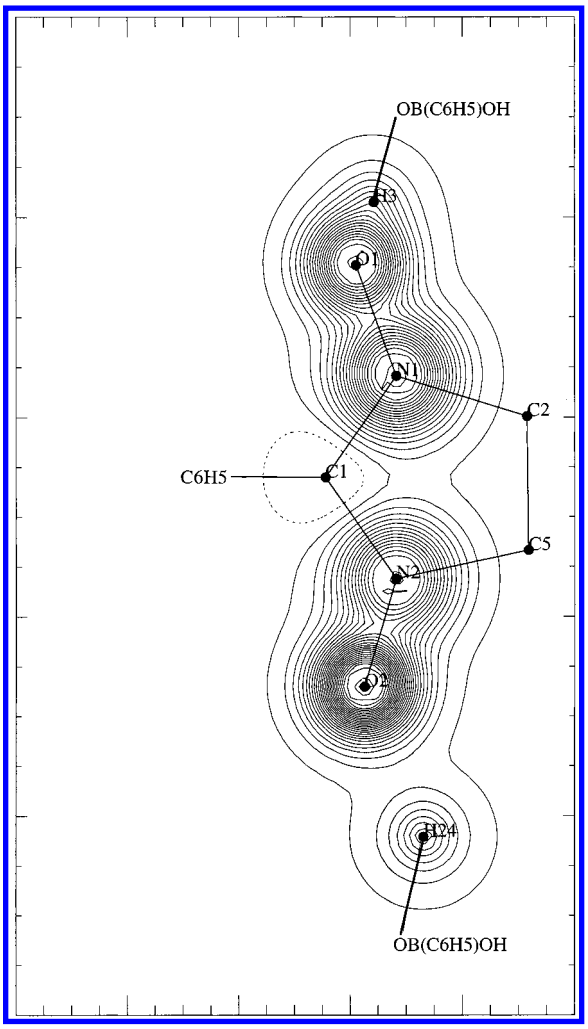

Figure 8. Projection onto the nitroxide mean plane of the spin density as analyzed by wave function modeling (PNNB). Negative contours are dashed: contours step 0.013 μ_B/Å^2.

Figure 8 shows the contours for the reconstructed spin density projected on the O−N−C−N−O molecular plane for one of the two radicals contained in the unit cell.

As expected from the MaxEnt results, most of the spin population is carried by the two NO groups of each radical. As in the other nitronyl nitroxide radicals, but not detected in the MaxEnt spin density map, the bridging sp^2 carbon atoms carry a negative spin density. Compared to the isolated case, some differences exist: on one hand, the O:N/N:O spin partitioning, which is approximately 1:1/1:1 for the isolated PNN, is 22:30/24:32 and 21:30/23:28, respectively, for O1:N1/N2:O2 and O22:

N22/N21:O21; a large unbalance is found between the two oxygen atoms of each radical. On the other hand, if the bridging carbon atoms C1 and C21 still carry a negative spin population, this density is weak (−0.025 (20) μ_B and −0.040 (22) μ_B) and far from the ratio of $-1/3$ (to the average of the spin populations of the O and N atoms) expected from previous studies.[14] Additionally, only the hydrogen atoms H4 (0.043 (22) μ_B) and H24 (0.055 (25) μ_B), atoms highlighted by the MaxEnt spin density reconstruction, and the boron atoms B1 (−0.067 (45) μ_B) and B2 (−0.037 (25) μ_B) carry significant spin populations.

In conclusion to the spin density reconstructions, we can say that the two approaches used here converge and give practically the same results for the two pairs of molecules comprised in the unit cell. The amount of the spin density on the two oxygen atoms of each radical is really different. Moreover, a positive spin density is found on the hydrogen atoms involved in the BOH···ON hydrogen bonds but mainly on one of the two hydrogen bonds that connect each of the PNN molecule. Thus, it seems that these hydrogen bonds play an important role in the ferromagnetic intermolecular interactions and are responsible for the peculiar spin density distribution of this radical.

Discussion and ab Initio Spin Density Calculations. As already mentioned, the $P2_1/n$ form of the PNNB undergoes a phase transition around 220 K. This transition is due to the ordering of the methyl groups of the five-membered ring. On cooling below this temperature, the space group changes to $P\bar{1}$. The main effect induced by this crystallographic transition is that the unit cell includes two crystallographic different pairs of molecules [(**1** + **2**) and (**1′** + **2′**)] instead of two equivalent pairs (**1** + **2**), with now four hydrogen bonds with significantly different geometries, as depicted below:

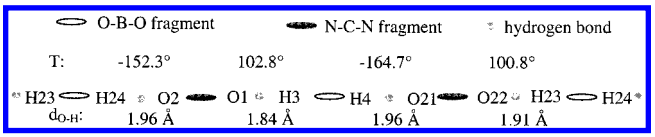

Both MaxEnt and wave function modeling methods agree and show that the spin density distribution is quite similar for the two pairs (**1** + **2**) and (**1′** + **2′**). Although the experimental results are less accurate than those generally obtained from polarized neutron experiments (due to the limitation to reflections (*h*0*l*)), the effects observed are significant and can be discussed at a quantitative level:

(i) Most of the spin density is concentrated on the nitronyl fragment and is located on the nitrogen and oxygen atoms. This contribution may be attributed to the unpaired electron residing on the singly occupied molecular orbital (SOMO) constructed on the $|2p\rangle$ atomic orbital of the O and N atoms.

(ii) Compared to the isolated PNN radical, the spin population is not symmetrically distributed between the two oxygen atoms of the nitronyl fragment: one of the two oxygen atoms is depleted in favor of the other. We have shown that this depletion is more effective on the oxygen atom involved in the shorter hydrogen bond: the spin density on O1 (O22), corresponding hydrogen bond length 1.84 Å (1.91 Å), is significantly less than on O2 (O21), corresponding hydrogen bond length 1.96 Å (1.96 Å). It is not the first time that this sort of spin density unbalance has been observed in organic radicals. It was already encountered in our polarized neutron diffraction studies of an inter-homomolecular hydrogen-bonding system.[12,13]

(iii) The hydrogen atoms of the phenyl boronic acids that are involved in the hydrogen bonds carry a spin density of the same sign as those carried by the NO groups. The stronger "transfer" of spin density corresponds to the longer hydrogen bonds: spin density on H3 (H23) is much less than on H4 (H24).

(iv) The spin polarization effect[30] (SP), generally observed on the bridging sp^2 carbon atom (negative spin density) in nitronyl nitroxide radicals previously studied, is found on the PNNB complex. However, the spin population found in the present case is less than that expected.

Table 3. DFT (DGAUSS) Theoretical Spin Populations Calculated for the Experimental Geometry (X-ray Diffraction, 143 K) of One of the Two Radical Connected to Two Phenyl Boronic Acids in Comparison with Experimental Values Scaled to 1μ_B/Formula

	isolated PNN	conected molecules	experiment
H3		−0.001	0.024 (36)
O1	0.290	0.253	0.227 (25)
N1	0.220	0.233	0.307 (25)
C1	−0.089	−0.101	−0.025 (20)
N2	0.224	0.252	0.246 (25)
O2	0.285	0.268	0.328 (25)
H24		0.002	0.056 (25)

To better understand the effect of the hydrogen bonds on the spin density distribution, we performed several ab initio calculations. There are two types of ab inito methods to calculate the spin densities of molecular compounds: (i) the Hartree−Fock (HF) and HF-based methods,[31] and (ii) the density functional theory (DFT) methods.[32] Zheludev et al.[14] have shown that, on one hand, the calculated spin densities obtained by DFT are very stable with respect to the choice of basis and functional sets, and on the other hand, they give results that are much closer to those experimentally determined. For these reasons, our calculations were performed using DFT method as implemented in the program DGAUSS.[33]

To get a reliable picture of the role of hydrogen bonds on the spin density of the radical, we have compared the calculation for an isolated PNN radical and the calculation for a PNN radical connected to two phenyl boronic acids. We have selected the pair where the difference between the two hydrogen bonds is the higher: H23−OBO−H24···O2−NCN−O1···H3−OBO−H4. These two calculations were performed for molecules in their low-temperature geometry, as determined by X-ray diffraction (T = 143 K).

The individual atomic Mulliken spin populations of the connected molecules and of the isolated radical are displayed in Table 3 together with experimental values scaled to 1 μ_B/PNN radical. First, one can note that in the isolated case, as previously described,[14] the DFT calculations give a similar spin population for the two NO groups: 0.510 μ_B for N1O1 and 0.509 μ_B for N2O2 with an equivalent population on the two oxygen atoms. However, as already mentioned in ref 14, the DFT does not yield for the isolated PNN the equality between the N and the O populations, which was found experimentally. Beside this, compared to the isolated case, when the molecules are in interactions, the two oxygen atoms O1 and O2 are depleted and this effect is more pronounced on the O1 atomic

(30) Nakaitsuji, I. *J. Chem. Phys.* **1973**, *59*, 2586.
(31) Moller, C.; Plesset, M. S. *Phys. Rev.* **1934**, *46*, 618. Shavitt, I. Methods of Configurational Interaction. In *Modern Theoretical Chemistry*; Shaefer, H. F., III, Ed.; Plenum Press: New York, 1977; Vol. 3, p 189.
(32) Kohn, W.; Sham, L. J. *Phys. Rev. A* **1965**, *1133*, 140.
(33) DGAUSS UniChem4, Cray Research Inc., Cray Research Park, 655 Lone Oak Drive, Eagan, MN 55121. At the local spin density functional level, the functional of Vosko, Wilk, and Nusair[34] was utilized, with the nonlocal correlational potential of Perdew'86[35] and the nonlocal exchange potential of Becke'88.[36] The different calculations were done with the TZ94+P basis set.
(34) Vosko, S. H.; Wilk, L.; Nausair, M. *Can. J. Phys.* **1980**, *58*, 1200.
(35) Perdew, J. P. *Phys. Rev. B* **1986**, *33*, 8822.
(36) Becke, A. D. *Phys. Rev. A* **1988**, *38*, 3098.

site: O1 changes from 0.290 μ_B to 0.253 μ_B and O2 changes from 0.285 μ_B to 0.268 μ_B. Thus, as experimentally observed, the stronger reduction is obtained on the oxygen atom involved in the shorter hydrogen bond. Furthermore, in the "interacting" case, a positive but very small spin population is obtained on the H24 hydrogen atom, the hydrogen atom for which the experiment gives a strong and a significant positive spin population. Finally, DFT calculations fail to predict correctly the amount of spin population residing on the central carbon atom C1: from the isolated case to the interacting case, the absolute value of this spin population increases rather substantially while experimentally it is quite low.

In conclusion to these ab initio spin density calculations, one can say that, on the whole, the experimental effects are "seen" by DFT calculations. However, although there is a good qualitative agreement, from the quantitative point of view, the DFT results are still very far from the experimental one. The calculated unbalance between the two oxygen atoms represents 6% of the average of the spin populations of the O1, N1, N2, and O2 atoms, instead of 36% experimentally, and the calculated "transfer" of spin density to the H24 atom is at least 1 order of magnitude less than the experimental one.

From a general point of view, it appears that the geometry of the hydrogen bond has a direct effect on the global spin density distribution of the complex. We have here direct evidence of the active role played by the hydrogen bonds in the intermolecular ferromagnetic coupling. We have shown that the intermolecular exchange pathway between the SOMO of each radical involves the diamagnetic molecule and is obtained via hydrogen bonds.

Conclusion

We have investigated, by polarized neutron diffraction, the spin density distribution in a very interesting case of interheteromolecular hydrogen-bonding system. This molecular complex allows the study of the effect of inequivalent hydrogen bonds on the global spin density distribution.

The main feature herein highlighted is the spin depletion on the oxygen atom of the NO groups of the PNN radical, due to the hydrogen bonds, and the unbalance induced by the difference in the hydrogen bond geometry. Shortest is the length of this bond (shortest is the torsion angle) and higher is the oxygen depletion. Another important point is the spin density transfer from the NO groups toward the hydrogen atoms of the hydrogen bond, but shortest is the distance (shortest is the torsion angle) and lowest is the transfer. This effect is seen by DFT calculations but at a level much lower than the level for that experimentally found.

Finally, both experimental spin density determination and ab initio calculations have shown that the hydrogen bonds are involved in the intermolecular exchange pathway, but the DFT calculations fail to predict quantitatively the experimental effects.

Acknowledgment. The financial support of MURST and TMR grant 3MD (No. ERB 4061 PL 97-0197) is gratfully acknowledged. Thanks are also expressed to Dr. A. Caneschi, Dr. R. Sessoli, and to Pr. D. Gatteschi, University of Florence, for helpful and stimulating discussions.

JA991042U